Progress In Electromagnetics Research, PIER 22, 107–129, 1999

A HYBRID FEM/BEM/WTM APPROACH FOR FAST SOLUTION OF SCATTERING FROM CYLINDRICAL SCATTERERS WITH ARBITRARY CROSS SECTIONS

Z. Xiang

Electromagnetic Laboratory
DSO National Laboratories
20 Science Park Drive, Republic of Singapore 118230

Y. Lu

School of Electrical and Electronic Engineering
Nanyang Technological University
Nanyang Avenue, Republic of Singapore 639798

1. INTRODUCTION

Many problems in electromagnetics involve scattering from arbitrarily shaped, inhomogeneous and lossy bodies. These problems can be divided into two groups, i.e., unbounded (or exterior) and bounded (or interior) problems. Some methods, for example, the FEM, are

suitable for the interior problems while such methods as the BEM are suited for the exterior problems [1]. A hybrid method combining the advantages of the above-mentioned methods is able to solve a more general class of problems [2–3]. The use of the FEM for the interior problems results in sparse matrices. However, the use of the conventional BEM for integral equations always results in full matrices. For convolutional boundary the fast Fourier transform (FFT), in conjunction with an iterative-solution approach, such as the conjugate-gradient (CG) or biconjugate-gradient (BiCG) method, can be used to efficiently evaluate the boundary integrals [2]. However, for many practical electromagnetic (EM) problems, for example, elongated structures involved, there does not exist a completely convolutional boundary integral, making the FFT not effective.

Recently, wavelet transform method (WTM) has been widely used for efficient solutions of EM integral equations because of its obvious advantages over Fourier-based techniques [4–9]. More recently, the authors presented a hybrid technique which combined the method of moments (MoM), the FEM and the WTM for efficient solutions of EM problems with arbitrarily inhomogeneous materials [10]. The equivalence principle was used to divide the original problem into the interior and exterior problems. The interior problem was efficiently solved by the FEM while the exterior problem was handled by the MoM. The WTM was used to speed the MoM solutions for the exterior problem.

In this paper, alternative hybrid method (called FEM/BEM/WTM approach) is proposed. The hybrid technique uses the FEM to formulate the fields within a fictitious boundary enclosing the considered structure and establish a relationship with those on the fictitious boundary. The fields outside the fictitious boundary are solved by the BEM involving an integral expression of the fields over the fictitious boundary. A system is then derived by enforcing field continuity across the boundary. To avoid solving the dense matrix equation from the BEM, two fast-solving techniques based on the WTM are presented. The use of the proposed hybrid technique always results in sparse moment matrices which can be efficiently solved by a sparse solver. Uniting the advantages of the FEM, BEM and WTM, the proposed hybrid technique can effectively handle unbounded problems in which *arbitrary* complex inhomogeneities are involved.

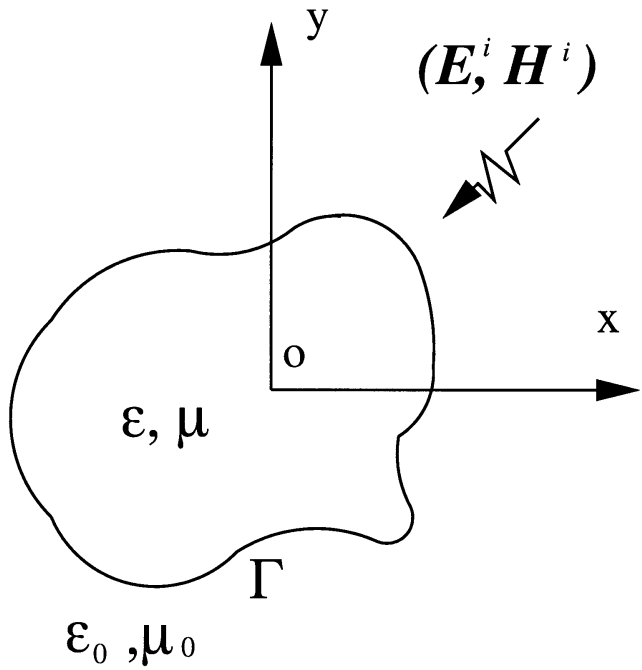

Figure 1. Scattering from a cylindrical scatterer of arbitrary shape.

2. FORMULATION

We consider the scattering from a cylindrical scatterer of arbitrary cross section as shown in Fig. 1. The dielectric properties of the scattering object are given as complex functions $\epsilon_r(\mathbf{r})$ and $\mu_r(\mathbf{r})$. Assume an electromagnetic wave is incident in the direction normal to the axis of the cylinder, i.e., the z-axis. Both TM (E-polarization) and TE (H-polarization) incident waves are considered, and $e^{i\omega t}$ time convention is assumed. Let the fictitious boundary be Γ enclosing the region of inhomogeneous dielectric cylinder. The region within the fictitious boundary Γ is the so-called interior region and referred to as region Ω_i, and the region outside the fictitious boundary Γ is the exterior region and referred to as region Ω_∞.

2.1 Finite Element Analysis for the Interior Region

To formulate the fields in the region Ω_i, we begin with the Helmholtz equation

$$\left[\frac{\partial}{\partial x}\left(\frac{1}{p}\frac{\partial}{\partial x}\right)+\frac{\partial}{\partial y}\left(\frac{1}{p}\frac{\partial}{\partial y}\right)+k_0^2 q\right]u=0,\quad (x,y)\in\Omega_i \tag{1}$$

where $u=E_z$, $p=\mu_r$ and $q=\epsilon_r$ for E-polarization, and $u=H_z$, $p=\epsilon_r$ and $q=\mu_r$ for H-polarization, respectively. $k_0=\omega\sqrt{\mu_0\epsilon_0}$ is the wavenumber in the free space. A traditional approach for solving (1) is to consider the functional

$$F(u)=\frac{1}{2}\int\!\!\int_{\Omega_i}\left[\frac{1}{p}\left(\frac{\partial u}{\partial x}\right)^2+\frac{1}{p}\left(\frac{\partial u}{\partial y}\right)^2-k_0^2 q u^2\right]d\Omega+\oint_\Gamma u\Psi d\Gamma \tag{2}$$

where $\Psi=jk_0Z_0(\mathbf{H}\times\hat{n})\cdot\hat{z}$ for E-polarization, and $\Psi=-jk_0Y_0(\mathbf{E}\times\hat{n})\cdot\hat{z}$ for H-polarization, respectively. It can be easily shown that the solution to (1) can be obtained by solving an equivalent variational equation via enforcing

$$\delta F(u)=0 \tag{3}$$

where $\delta F(u)$ denotes the first-order variation of F about u. To discretize the functional (2), the interior region Ω_i is subdivided into N small triangular or quadrilateral elements, and consequently, the fictitious boundary Γ is broken into M_s short segments. On the assumption that the field distribution within each element is linear, or quadratic, or higher order function, the field of the e-th element can be expressed as

$$u^e(x,y)=\sum_{i=1}^{3n}N_i^e(x,y)\,u_i^e \tag{4}$$

where $N_i^e(x,y)$ is the interpolation function, u_i^e represents the nodal field and n stands for the order of the interpolation function. For the discretization of the line integral in (2), on the s-th segment of the fictitious boundary Γ, the field can be expressed as

$$u^s(x,y)=\sum_{i=1}^{2m-1}N_i^s(x,y)\,u_i^s \tag{5}$$

where $N_i^s(x,y)$ represents the shape function for the s-th segment, u_i^s denotes the nodal field on the fictitious boundary, and m defines the order of the shape functions. Furthermore, assuming that the fictitious

boundary Γ is smooth contour, the Ψ is well defined at each nodal on Γ and can be expressed as

$$\Psi^s(x,y) = \sum_{i=1}^{2m-1} N_i^s(x,y)\,\Psi_i^s \tag{6}$$

Substituting (4)–(6) into (2) and applying the Galerkin's procedure to enforce (3), we can obtain a system of equations as follows:

$$Ku + C\Psi = 0 \tag{7}$$

where u and Ψ are the column vectors to be solved, and the elements in matrices K and C are given by

$$K_{ij}^e = \iint_{\Omega_i^e} \left\{ \frac{1}{p^e} \left[\frac{\partial N_i^e}{\partial x}\frac{\partial N_j^e}{\partial x} + \frac{\partial N_i^e}{\partial y}\frac{\partial N_j^e}{\partial y} \right] - k_0^2 q^e N_i^e N_j^e \right\} dx\, dy, \tag{8}$$

$$C_{ij}^s = \oint_{\Gamma^s} N_i^s N_j^s d\Gamma \tag{9}$$

2.2 Boundary Element Analysis for the Exterior Region

As we know, at the fictitious boundary the electric and magnetic fields satisfy the continuity conditions as follows:

$$u_{in} = u_{ex}, \qquad \frac{1}{p}\frac{\partial u_{in}}{\partial n} = \frac{\partial u_{ex}}{\partial n} \qquad \text{on } \Gamma \tag{10}$$

which are realized by the following boundary integral equation

$$u(\mathbf{r}) = u^{inc}(\mathbf{r}) + \oint_\Gamma \left[u(\mathbf{r}') \frac{\partial G_0(\mathbf{r},\mathbf{r}')}{\partial n'} + G_0(\mathbf{r},\mathbf{r}')\,\Psi(\mathbf{r}') \right] d\Gamma' \tag{11}$$

where $u^{inc}(r)$ stands for the incident field and G_0 denotes the two-dimensional Green's function in the free space. G_0 is expressed in term of the zeroth-order Hankel function of the second kind as follows:

$$G_0(\mathbf{r},\mathbf{r}') = \frac{1}{4j} H_0^{(2)}\left(k_0|\mathbf{r}-\mathbf{r}'|\right) \tag{12}$$

Substituting (5) and (6) into the boundary integral equation (11) and applying Galerkin's procedure, we obtain the matrix equation as follows:

$$C^T u = B + Pu + Q\Psi \tag{13}$$

where T denotes the transpose of a vector, the matrix elements of C are the same as those in (9), and the other matrix elements are given by

$$P_{ij}^{st} = \oint_{\Gamma^s} N_i^s(x,y) \left[\oint_{\Gamma^t} N_j^t(x',y') \frac{\partial G_0(\mathbf{r},\mathbf{r}')}{\partial n'} d\Gamma' \right] d\Gamma, \tag{14}$$

$$Q_{ij}^{st} = \oint_{\Gamma^s} N_i^s(x,y) \left[\oint_{\Gamma^t} N_j^t(x',y') G_0(\mathbf{r},\mathbf{r}') d\Gamma' \right] d\Gamma, \tag{15}$$

$$B_i^s = \int_{\Gamma^s} N_i^s u^{inc} d\Gamma, \tag{16}$$

where s, $t = 1, 2, 3, ..., M_s$. The combined system of (7) and (13) now forms a complete system equation, i.e.,

$$AX = B_0 \tag{17}$$

where

$$A = \begin{bmatrix} K & C \\ P_0 & -Q \end{bmatrix}, \quad X = \begin{pmatrix} u \\ \Psi \end{pmatrix}, \quad B_0 = \begin{pmatrix} \phi \\ B \end{pmatrix}, \tag{18}$$

where $P_0 = C^T - P$ and ϕ is a $M \times 1$ zero matrix. A is a square matrix of order $M + M_s$, in which the sub-matrix K is a $M \times M$ square matrix; C is a $M \times M_s$ rectangular matrix; P_0 is a $M_s \times M$ rectangular matrix; Q is a $M_s \times M_s$ square matrix where M and M_s denote the total node number and boundary node number respectively. Both B and Ψ are the column vectors of M_s elements, and u is a column vector of M elements.

To minimize the computation, the fictitious boundary should be carefully chosen. First of all, in order to minimize the FEM computation for the interior problem and the BEM computation for the exterior problem, the fictitious boundary should be chosen to make the interior region as small as possible. Secondly, the fictitious boundary should be as smooth as possible to obtain the most sparse moment matrix while using the WTM. This is because the smoother the integral boundaries, the sparser the moment matrices by using wavelet transforms

[8]. Notice that the system matrix A in (18) is only dependent of the structure of the scatterer, which means that one only need to evaluate A once to solve the scattering problem by different incident fields.

2.3 Wavelet Transforms for Effective Solution of Boundary Integral Equations

As mentioned above, the FEM for the interior problem results in a very sparse matrix. However, using the traditional basis and weighting functions to deal with the boundary integral by using the BEM always generates a dense matrix. In this paper, the wavelet matrix transform (WTM) method [11–14] is used to overcome the difficulties. An effective wavelet transform basis matrix is specially constructed for our problem. Using the constructed wavelet matrix, one can transform the partly-full matrix to a completely sparse one which can be efficiently solved by a sparse solver.

Wavelet theory is one of the systematic and rapidly developing mathematic branches. It is not possible to give a complete description here because of the limited space. A compact version of description for the wavelet theory is given in the Appendix. More knowledge about the wavelet theory can be found in [11–13].

For our problem we propose two fast-solving ways based on the WTM. The two solving procedures are compared by solving the same EM problem in numerical experiment section. Their advantages will be revealed and compared. Non-orthonormal cardinal spline wavelets (NCSW) [12, 13] are used. It has been shown by the author [9] that a non-similarity wavelet transform, for example, non-similarity NCSW (NS-NCSW) transform, could obtain much higher compression rate for the same threshold and much better accuracy for the same compression rate than a similarity wavelet transform such as Daubechies' orthonormal wavelet (DOW) for EM problems. The first way is to directly solve equation (17) by using wavelet matrix transform method [9]. However, a specific wavelet basis matrix has to be constructed for equation (17). Notice that the sub-matrices Q and P are generated from the integrals with kernels $H_0^{(2)}(k_0|\mathbf{r}-\mathbf{r}'|)$ and $H_1^{(2)}(k_0|\mathbf{r}-\mathbf{r}'|)$, respectively; the basis and weighting functions in the BEM are generally chosen to be linear or quadratic. Therefore, it is enough to choose 8-order vanishing moment of the wavelets for the considered problems. Let $\tilde{U}$ be the $M_s \times M_s$ wavelet basis matrix constructed by the method in [9], and define a $(M+M_s)\times(M+M_s)$ square matrix W for equation

(17) as follows:

$$W = \begin{bmatrix} I & \phi_1 \\ \phi_2 & \tilde{U} \end{bmatrix} \tag{19}$$

where I stands for the $M \times M$ unit matrix, ϕ_1 the $M \times M_s$ zero matrix and ϕ_2 the $M_s \times M$ zero matrix. Applying the constructed wavelet matrix W to transform (17) one can obtain a completely sparse matrix equation as follows:

$$A'X' = B'_0 \tag{20}$$

where $X' = \left(W^T\right)^{-1} X$, $B'_0 = WB_0$ and $A' = WAW^T$. X' in (20) can be efficiently solved by a sparse solver. Once X' is solved, one can use the reconstruction algorithm of the wavelets to obtain the needed result for our problem, i.e., $X = W^T \left(W^T\right)^{-1} X = W^T X'$.

Another efficient way is possible if one observes the matrix equation (17) carefully and carries out a simple matrix manipulation. Instead of directly dealing with a combination matrix equation (17), we first factorize the banded sparse matrix K in (7) from the FEM to obtain the expression of u as follows:

$$u = -K^{-1}C\Psi, \tag{21}$$

then substitute u into (13) to obtain a smaller-size matrix equation with matrix variable Ψ as follows:

$$A\Psi = B, \tag{22}$$

where

$$A = \left(P - C^T\right) K^{-1}C - Q. \tag{23}$$

Note that in this case the order of matrix A is equal to the number of the discretized points on the fictitious boundary, and A is a full matrix. Furthermore, C is trivial matrix and K is a regular matrix. From the expression of A in (23) we know that the singularity property of dense matrix A is completely determined by the properties of both dense matrices P and Q because A is only a linear combination of P and Q. According to the recommendation in [9] one can obtain a good compression rate with at least single precision approximate solutions if choosing 8-order vanishing moment of wavelets for wavelet transforms.

Here, we can directly apply the wavelet basis matrix $\tilde{U}$ to transform (23) to obtain

$$\left[A'\right]\{\Psi'\} = \{B'\} \tag{24}$$

where $\Psi' = \left(\tilde{U}^T\right)^{-1}\Psi$, $B' = \tilde{U}B$ and $A' = \tilde{U}A\tilde{U}^T$. For a given threshold value A' is a sparse matrix, and therefore, Ψ' in (24) can be efficiently solved by a sparse solver. Once Ψ' is solved, one can use the reconstruction algorithm of the wavelets to obtain Ψ, i.e., $\Psi = \tilde{U}^T\left(\tilde{U}^T\right)^{-1}\Psi = \tilde{U}^T\Psi'$. Finally, substituting Ψ into (21) one can obtain u. Once the values of u and Ψ on the fictitious boundary Γ are solved, one can use them to compute the interested RCS.

2.4 Formulation for Radar Cross Section (RCS)

For our problem, the interested parameter is the radar cross section (RCS) which is defined by

$$\sigma = \lim_{r\to\infty}\left(2\pi r\frac{|\mathbf{E}_s|^2}{|\mathbf{E}^i|^2}\right) \tag{25}$$

for the TM case, and by

$$\sigma = \lim_{r\to\infty}\left(2\pi r\frac{|\mathbf{H}_s|^2}{|\mathbf{H}^i|^2}\right) \tag{26}$$

for the TE case. For the considered problems, it can be evaluated as follows:

$$\sigma = \frac{4}{k_0}|\mathbf{P}(\varphi)|^2 \tag{27}$$

where φ is observation angle and $P(\varphi)$ is the far-field coefficient given by

$$P(\varphi) = \frac{1}{4}\oint_\Gamma\left[\Psi + ik_0u(\hat{n}\cdot\hat{r})\right]e^{ik_0(x\cos\varphi + y\sin\varphi)}d\Gamma \tag{28}$$

where $\hat{n}$ and $\hat{r}$ denote the normal unit vector on Γ and the unit vector in the direction of the observation, respectively. Substituting the values of u and Ψ on the fictitious boundary Γ into (28), one can compute the interested RCS.

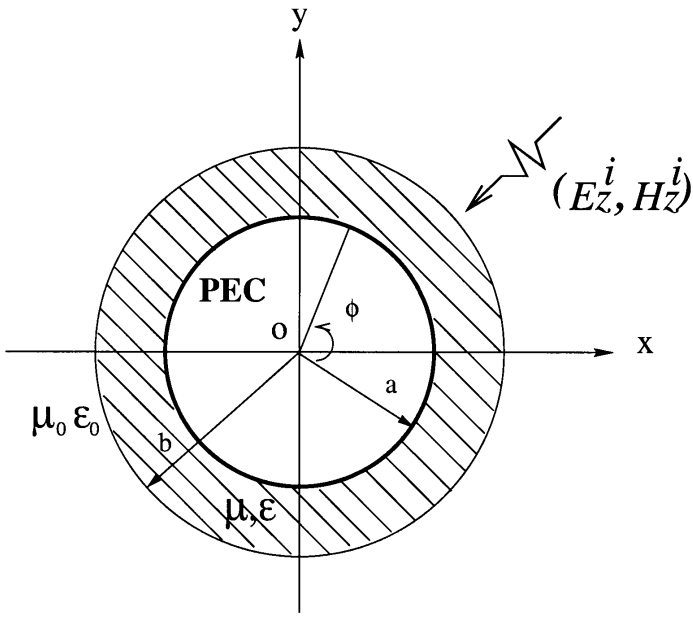

Figure 2. Scattering from a coated conducting cylinder.

3. NUMERICAL RESULTS

In this section, we will show the validity and the effectiveness of the proposed hybrid FEM/BEM/WTM method by the numerical examples.

We first consider the scattering from a coated conducting circular cylinder, shown in Fig 2. The parameters of the scatterer are given as follows: the relative permittivity $\epsilon_r = 4 - 4i$; the relative permeability $\mu_r = 1$; the outer radius $b = 3.0\lambda_0$; the inner radius $a = 2.9\lambda_0$, where λ_0 is the wavelength in the free space. Assuming a plane wave is excited, and the incident angle $\varphi_i = 0$.

To minimize the computation, the fictitious boundary Γ is chosen to be the natural boundary of the structure, i.e., the outer boundary. Since the boundary integral is convolutional, it is only necessary to compute, respectively, one row or column of the sub-matrices P and Q in (13), thus reducing the computing time significantly to form the complete system equation (17).

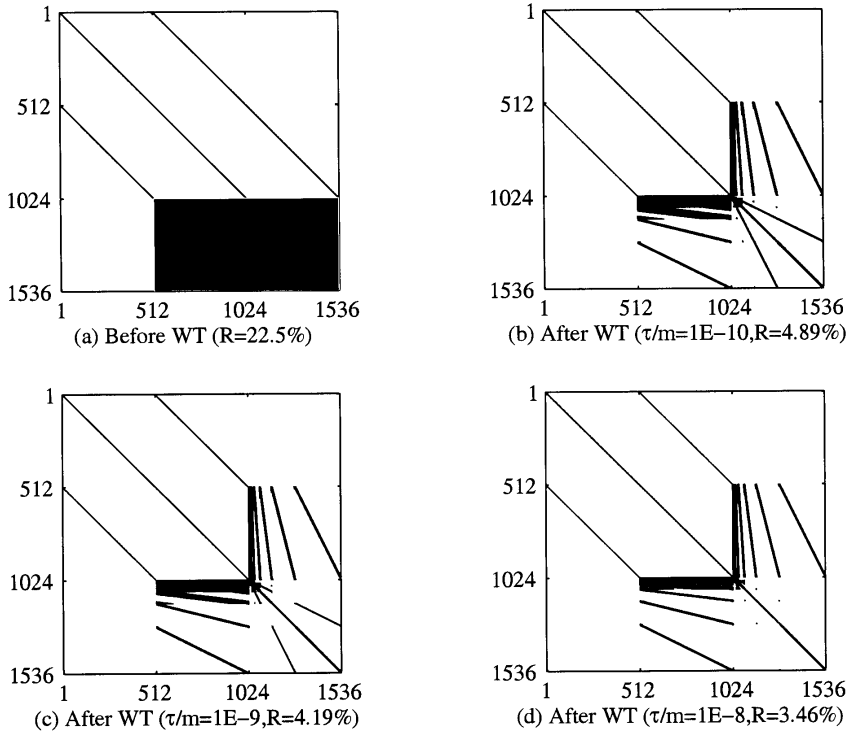

Figure 3. The remaining nonzero elements by using the first method after setting to zero each element whose magnitude is smaller than a selected threshold τ. (a) shows A before the WTM, and (b)–(d) show A' with different threshold values after the WTM.

We discretize the interior region, i.e., the coated layer, into small triangular elements by dividing the radial direction into 2 equi-thickness layers and the angular direction into 512 equal segments, i.e., $M_s = 512$. Fig 3 shows non-zero element distributions of the resultant matrices A from (17) and A' from (20) by setting the threshold $\tau/m = 10^{-10}$, 10^{-9} or 10^{-8} for the TM case, where m stands for the largest magnitude of the elements in A'. The black dots represent the remaining nonzero elements and R stands for the ratio of number of the remaining nonzero elements to the total elements. In Fig. 3(a), there are two 512×512 full sub-matrices which are generated from the boundary integral equation. They become sparse by wavelet transform after setting even a small threshold value, as shown in Fig. 3(b)–(d).

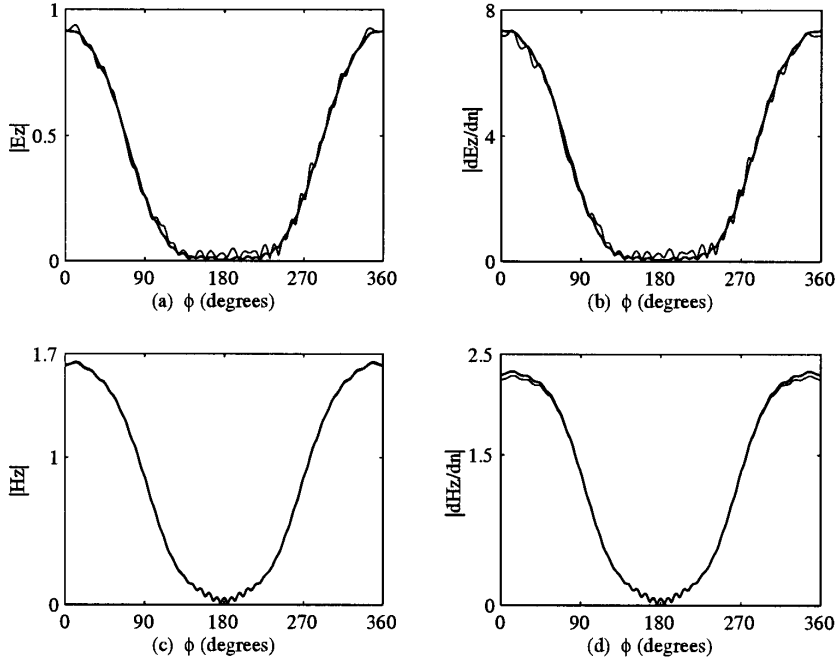

Figure 4. Distributions of fields and their normal derivatives on Γ for the conducting cylinder coated with lossy material ($\mu_r = 1$ and $\epsilon_r = 4 - 4i$) obtained by using the first method. The thicker line: the analytical solution; the thin line: the WTM solution. (a) and (b) for TM wave incidence $(\tau/m = 1E - 8)$, and (c) and (d) for TE wave incidence $(\tau/m = 1E - 7)$.

Figure 4 gives the distribution of the fields and their normal derivatives, and Fig. 5 shows the RCSs of the scatterer for TM and TE incidence, respectively. Even with so sparse matrices A's ($R = 3.46\%$ for TM incidence and $R = 3.51\%$ for TE incidence) can the hybrid method obtain an accurate solution by a sparse solver.

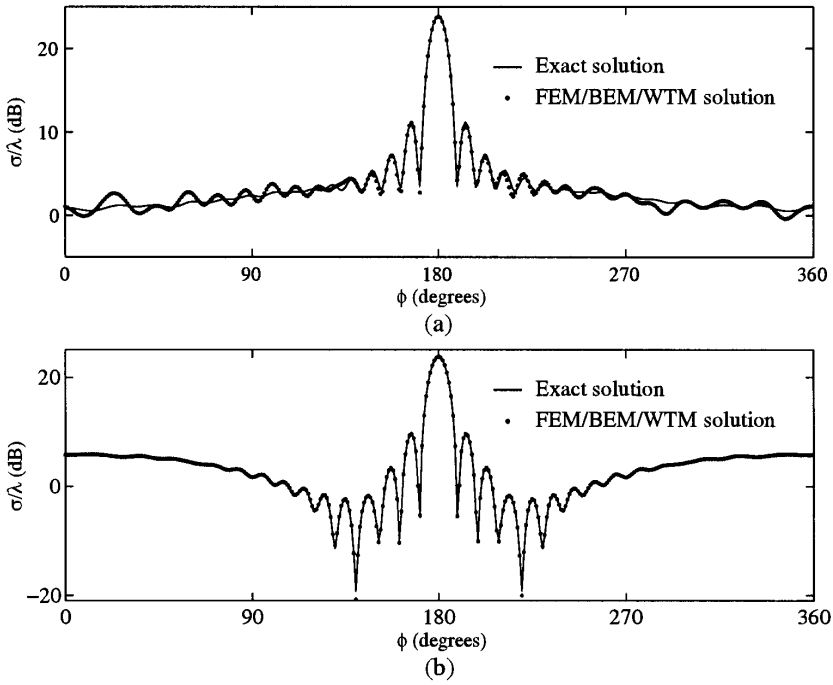

Figure 5. RCS for the conducting clyinder coated with lossy material ($\mu_r = 1$ and $\epsilon_r = 4-4i$) obtained by using the first method. (a) under TM wave incidence ($\tau/m = 1E-8$); (b) under TE wave incidence ($\tau/m = 1E-7$).

Fig. 6 shows non-zero element distributions of A' in (24) obtained by the second wavelet transform way by setting the threshold $\tau/m = 10^{-6}$ or $10^{-5.5}$ for both the the TM and the TE cases, where m stands for the largest magnitude of the elements in A'. The black dots represent the remaining nonzero elements and R stands for the ratio of number of the remaining nonzero elements to the total elements. Obviously, the moment matrices by the second wavelet transform method are much sparser than those by the first wavelet transform method.

Fig. 7 shows the RCSs by using the second method for TM and TE incidences, respectively. Even with so sparse matrices A's ($R = 2.14\%$ for both TM and TE incidences), the second wavelet transform method can obtain solutions with relative errors much less than 1% by a sparse solver.

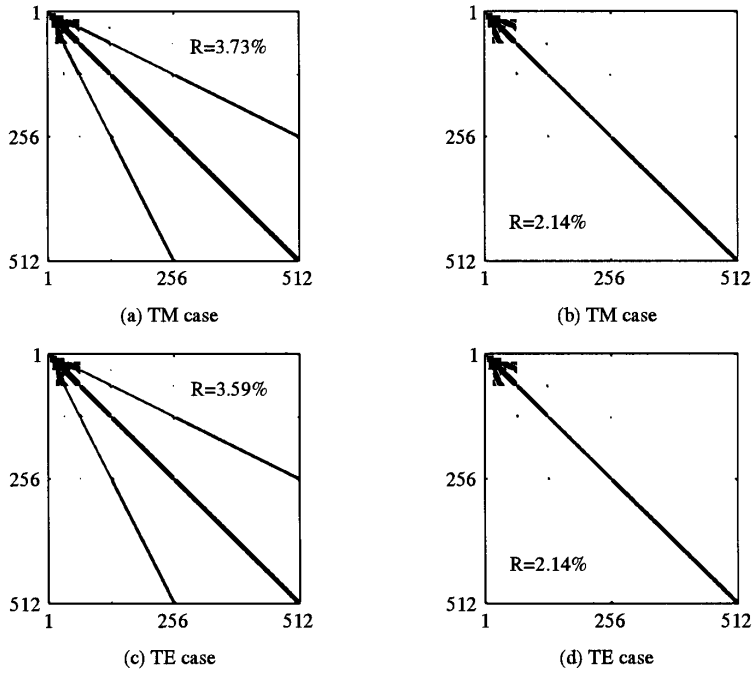

Figure 6. The remaining nonzero elements of A' by using the second method after setting to zero each element whose magnitude is smaller than a selected threshold τ. (a) and (c) $\tau/m = 10^{-6}$. (b) and (d) $\tau/m = 10^{-5.5}$.

It can be observed from Fig. 6 and Fig. 7 that using the second method one can obtain more accurate solutions for both TM and TE cases by only inverting two smaller-size and sparser matrices K (order 1024 and $R = 0.49\%$) and A' (order 512 and $R = 0.49\%$) compared with those by using the first method where one relatively large sparse matrix equation with order 1536 and $R = 3.46\%$ (for TM case) or $R = 3.51\%$ (for TE case) has to be inverted.

To demonstrate the effectiveness and the capacity of the proposed hybrid technique, another more complex electromagnetic scattering problem is considered. The geometry of the problems under analysis is shown in Fig. 8. The scatterer consists of two parts: the upper part is a semi-elliptical conducting cylinder whose major and minor axes are measured as a and b, respectively; the lower part is a semi-circular cylinder with radius b. A notch with depth h and ϕ is symmetrically

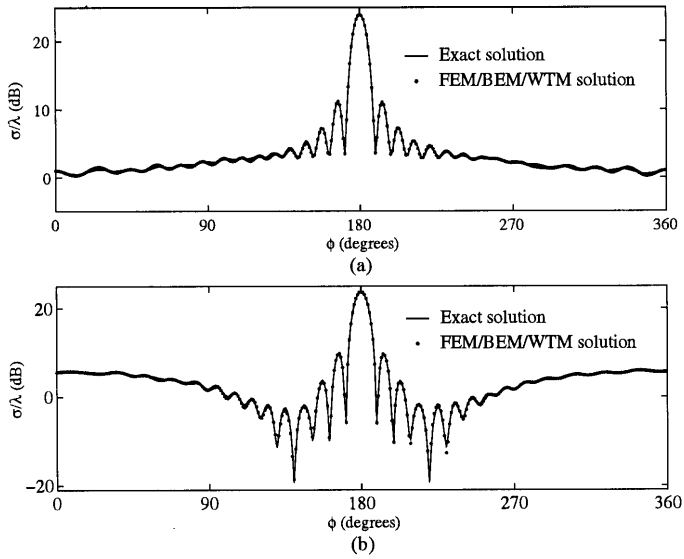

Figure 7. RCS for the conducting cylinder coated with lossy material ($\mu_r = 1$ and $\epsilon_r = 4 - 4i$) by using the second method. (a) under TM wave incidence ($\tau/m = 1E - 5.5$); (b) under TE wave incidence ($\tau/m = 1E - 5.5$).

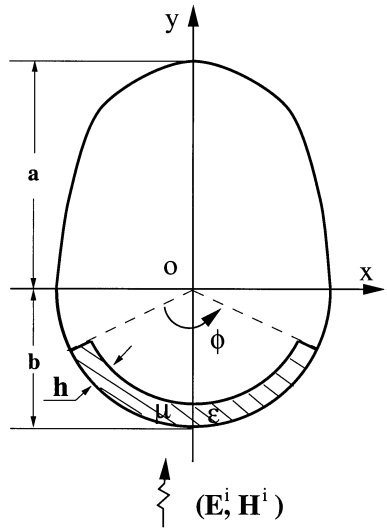

Figure 8. The geometry of the second problem under analysis. $a = \frac{40.63}{\pi}\lambda$, $b = \frac{20}{\pi}\lambda$, $\epsilon_r = 2.5(1-0.01i)$, $\mu_r = 1.0$, $f = 5GHz$, $h = 0.3\lambda$, $\phi = \pi.2$, $\varphi_i = -\pi/2$, under TM plane wave incidence.

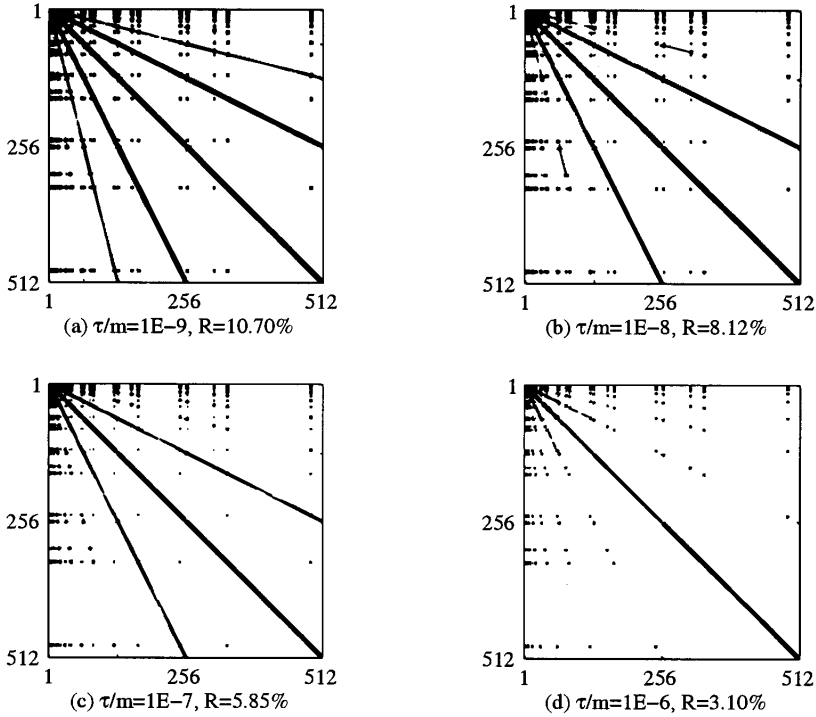

Figure 9. The remaining nonzero elements of A' for the second problem under analysis by using the second method after setting to zero each element whose magnitude is smaller than a selected threshold τ for the TM case.

located on the surface of the lower part and filled with complex media with the permittivity ϵ and the permeability μ.

For this problem, there is no analytical solution. we use the second wavelet transform method to solve it. The surface of the whole scatterer is chosen as the fictitious boundary and divided into 512 segments in equal radian. This discretization scheme will results in no more singularities. From this scheme we can obtain a satisfactory compression rate for the moment matrix by using the WTM [8]. Along the radial of the notch we divide the coated medium into three equal-space layers.

Fig. 9 shows non-zero element distributions of A' in (24) by setting the threshold $\tau/m = 10^{-9}$, 10^{-8}, 10^{-7} and 10^{-6} for the TM case. For the TE case, a similar sparse pattern can be achieved by the NS-NCSW transform method. It can be observed from Fig. 9 that for such

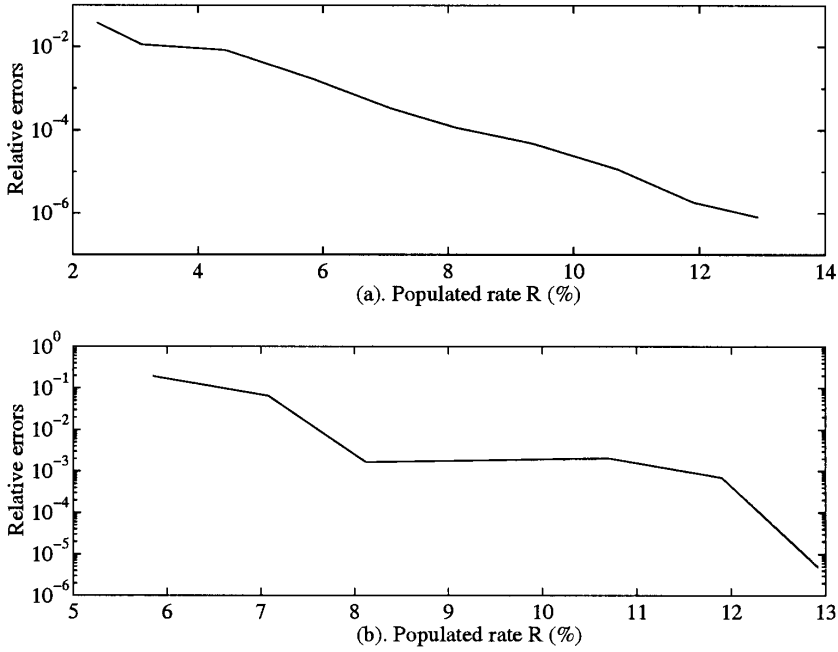

Figure 10. The relative error of solutions by the NS-NCSW transforms versus the populated rate R for the second problem under analysis. Reference solution is solved from the relevant dense matrix equation. (a). for u (b). for Ψ.

kinds of complicated EM problems one can still obtain a high compression rate by setting a small threshold τ/m. Compared with the sparse pattern in Fig. 6, as expected, the sparse pattern for this problem has a relatively less sparsity. This less sparsity results from wider range of radii of curvature of the fictitious boundary and more inhomogeneities. Nevertheless, one can still obtain accurate solutions to this problem by solving a sparse matrix equation with high compression rates.

Fig. 10 shows the solution accuracy of the surface magnetic field (denoted by Ψ) and electric field (denoted by u) by the proposed hybrid technique, compared with the results by the FEM/BEM method. It can be observed that in a wide range of populated rates one can obtain accurate solutions with relative errors less than 1% by sparse solvers.

Unlike the other traditional hybrid methods based on the FFT technique, the proposed hybrid technique can solve a wide range of EM problems without restriction on the shape or inhomogeneity of the scatterer or absorber. Furthermore, unlike the finite element solution using absorbing boundary conditions, the reliability of the hybrid method is independent of the scatterer's shape and composition and the polarization of the field. Provided that the finite element mesh is sufficiently fine and the proper threshold value is chosen in the WTM, the results always approach the true solutions. By controlling the threshold value in the WTM, one can flexibly trade off efficiency and accuracy.

4. CONCLUSIONS

In this paper, a hybrid FEM/BEM/WTM method has been proposed. The hybrid method employs the FEM to formulate the fields within a fictitious boundary enclosing the considered structure and establish a relationship with those at the opening. The fields outside the fictitious boundary are formulated by the BEM involving an integral expression of the fields over the fictitious boundary. Two wavelet transform basis matrices have been constructed and used to efficiently speed the solutions of boundary integral equations. The use of the proposed hybrid technique always results in sparse matrices which can be efficiently solved by a sparse solver. It has be shown in the literature that using the WTM one can obtain a solution in about or less than $O(N \log N)$ operations, where N is the number of unknowns in the discretized boundary integral equation. This is in contrast with a cost of $O(N^3)$ for a dense matrix inversion or $O(N^2)$ per dense matrix-vector multiplication in an iterative solution such as conjugate-gradient.

Combining the advantages of the FEM, BEM and WTM, the hybrid technique is able to effectively handle unbounded problems in which complex inhomogeneities are involved. For larger-size EM problems, the hybrid technique is much more effective than the traditional approaches. Furthermore, by controlling the threshold value in the proposed hybrid method, one can flexibly trade off efficiency and accuracy at different stages of analysis. Future efforts will be directed to the problems involving perfect conductors and arbitrarily shaped three-dimensional structures.

It deserved to be emphasized that both the hybrid FEM/BEM/WTM method and the FEM/MoM/WTM method [8] have very similar properties. First of all, both hybrid methods divide the original

problems into two problems. The former divides the original problems into the exterior and the interior problems which share the continuity conditions on the fictitious boundary; the latter divides the original problems into two problems by the equivalent current principle. Secondly, both hybrid methods form the so called interior problem which is efficiently solved by the FEM and an integral equation for the so called exterior problem which is effectively solved by the WTM and the BEM or the MoM. The differences between the two hybrid methods are the *different Green's functions* for the integral equations and the *different boundary value problems* for the interior problems. The computational complexities for both hybrid methods will keep the same level. Therefore, one can use either the FEM/BEM/WTM method or the FEM/MoM/WTM method to solve the same EM problems. The favourite formulations for the problems under analysis will determine the choice of the hybrid method.

APPENDIX: WAVELET THEORY

Wavelets are the functions that satisfy certain mathematic requirements. The very name *wavelet* comes from the requirement that they should integrate to zero, "waving" above and below the x-axis. There are many kinds of wavelets. One can choose among smooth wavelets, compactly supported wavelets, wavelets with simple mathematical expressions, wavelets with simple associated filters, etc. According to the projection relation among the chosen wavelets, we can divide wavelets into two kinds, i.e., the *orthogonal* and *non-orthogonal* wavelets. The latter is also referred to as the *biorthogonal* wavelets. Here, we only describe the the essentials of the theory of wavelets. More details about wavelets can be found in [11]–[13].

A.1 Orthonormal Wavelets

Define two functions $\phi(x)$ and $\psi(x)$ ($\phi(x), \psi(x) \in L^2(R)$) as follows:

$$\phi(x) = \sqrt{2} \sum_{n \in Z} h_n \phi(2x - n), \tag{A1}$$

$$\psi(x) = \sqrt{2} \sum_{n \in Z} g_n \phi(2x - n), \tag{A2}$$

where $g_n = (-1)^{1-n} h_{1-n}$. $\phi(x)$ and $\psi(x)$ are called scaling func-

tion and wavelet function, respectively. The sequence $\{h_n\}$ is called the filter sequence for the scaling function ϕ, and $\{g_n\}$ the filter sequence for the wavelet function ψ. For good approximation and data compression, the filter sequence for ψ is chosen so that it has certain number of vanishing moments, i.e.,

$$\sum_{n\in Z} n^j g_n = 0, \quad j = 0, ..., N-1, \tag{A3}$$

for some positive integer N. Furthermore, for orthonormal wavelets, the translations $\{\phi(x-n)|n \in Z\}$ and $\{\psi(x-n)|n \in Z\}$ are orthonormal if and only if

$$\sum_{n\in Z} h_n h_{n-2k} = \delta_{0,k}, \quad k \in Z, \tag{A4}$$

where $\delta_{0,k}$ is the Kronecker delta function defined with respect to k.

The filter coefficients of DOW are solved by requiring $h_n = 0$ ($n \neq 0, 1, 2m-1$) and $\{g_n\}$ to have m vanishing moments. Generally, these filter coefficients can only be solved numerically. More details can be found in Daubechies' book [11].

A.2 Non-orthonormal Wavelets

Unlike orthonormal wavelet algorithms, there are two scaling functions $\phi(x)$ and $\tilde{\phi}(x)$ for non-orthonormal wavelet algorithms [12], [13]. Since $\phi(x)$ and $\tilde{\phi}(x)$ are in V_1, they can be expressed in the following forms:

$$\phi(x) = \sqrt{2}\sum_{n\in Z} \tilde{a}_n \phi(2x-n), \tag{A5}$$

$$\phi(x) = \sqrt{2}\sum_{n\in Z} a_n \tilde{\phi}(2x-n), \tag{A6}$$

$$\tilde{\phi}(x) = \sqrt{2}\sum_{n\in Z} \tilde{p}_n \phi(2x-n), \tag{A7}$$

$$\tilde{\phi}(x) = \sqrt{2}\sum_{n\in Z} p_n \tilde{\phi}(2x-n), \tag{A8}$$

where $\{a_n\}$, $\{\tilde{a}_n\}$, $\{p_n\}$ and $\{\tilde{p}_n\}$ are called the filter coefficients for the scaling functions.

Unlike the orthonormal case, there correspond four wavelet functions $\psi(x)$, $\tilde{\psi}(x)$, $\eta(x)$, $\tilde{\eta}(x)$ which are defined by

$$\psi(x) = \sqrt{2}\sum_{n\in Z}\tilde{b}_n\phi(2x-n), \tag{A9}$$

$$\tilde{\psi}(x) = \sqrt{2}\sum_{n\in Z}q_n\tilde{\phi}(2x-n), \tag{A10}$$

$$\tilde{\eta}(x) = \sqrt{2}\sum_{n\in Z}\tilde{q}_n\phi(2x-n), \tag{A11}$$

$$\eta(x) = \sqrt{2}\sum_{n\in Z}b_n\tilde{\phi}(2x-n), \tag{A12}$$

where

$$\tilde{b}_n = (-1)^{1-n}a_{1-n}, \qquad b_n = (-1)^{1-n}\tilde{a}_{1-n},$$
$$\tilde{q}_n = (-1)^{1-n}p_{1-n}, \qquad q_n = (-1)^{1-n}\tilde{p}_{1-n}.$$

Like g_n in the orthonormal case, the filter sequences $\{\tilde{b}_n\}$, $\{b_n\}$, $\{\tilde{q}_n\}$ and $\{q_n\}$ are chosen so that they have certain numbers of vanishing moments to satisfy (31). The biorthogonal conditions satisfy (32) by replacing h_n and h_{n-2k} with $\tilde{a}_n$ and p_{n-2k}, or by replacing h_n and h_{n-2k} with a_n and $\tilde{p}_{n-2k}$, respectively.

Note that each of the sets $\{\psi_{0,n}|n\in Z\}$, $\{\tilde{\psi}_{0,n}|n\in Z\}$, $\{\eta_{0,n}|n\in Z\}$ and $\{\tilde{\eta}_{0,n}|n\in Z\}$ forms a basis for W_0. Furthermore, $\{\psi_{0,n}|n\in Z\}$ and $\{\tilde{\psi}_{0,n}|n\in Z\}$, and $\{\eta_{0,n}|n\in Z\}$ and $\{\tilde{\eta}_{0,n}|n\in Z\}$ are biorthogonal bases, respectively. The functions ψ and η and their duals $\tilde{\psi}$ and $\tilde{\eta}$ are called *non-orthonormal wavelets*. Various cases of multiresolution analysis can be obtained by combining one of the scaling functions and one of the wavelet functions.

If $\{\phi_{0,n}|n\in Z\}$ is an orthogonal basis of V_0, then $\phi=\tilde{\phi}$, $a_n=\tilde{a}_n=p_n=\tilde{p}_n$ for all $n\in Z$, and $\psi=\tilde{\psi}=\eta=\tilde{\eta}$. Therefore, the orthonormal wavelet is a specific one of the non-orthonormal wavelets.

One of the most attractive non-orthonormal wavelets is Non-orthonormal Cardinal Spline Wavelet (NCSW). The two scaling functions of NCSW are defined from the uniform B-spline of order k, i.e., $N_k(x)$, with $suppN_k=[0,k]$ [15]. NCSW has several remarkable features. For one thing, all the filter coefficients are dyadic rationales. Since division by 2 can be done very fast by a computer, this makes them very suitable for fast computations. Another attractive property is that the scaling functions and wavelets are known exactly and

explicitly for all x. Furthermore, each of the filter sequences for the NCSW has k-order vanishing moments which are important to obtain satisfactory data compression rates and solution accuracies. More details can be found in [12, 13].

REFERENCES

1. Sadiku, M. N. O., *Numerical Techniques in Electromagnetics*, Boca Raton: CRC Press, Inc., 1992.
2. Collins, J. D., J. M. Jin, and J. L. Volakis, "A combined finite element-boundary element formulation for solution of two-dimensional problems via CGFFT," *Electromagnetics,* Vol. 10, No. 4, 423–437, 1990.
3. Gong Z., and A. W. Glisson, "A hybrid equation approach for the solution of electromagnetic scattering problems involving two-dimensional inhomogeneous dieletric cylinders," *IEEE Trans. Antennas Propag.,* Vol. 38, No. 1, 60–68, Jan. 1990.
4. Steinberg, B. Z., and Y. Leviatan, "On the use of wavelet expansions in the method of moments," *IEEE Trans. Antennas Propag.,* Vol. 41, No. 5, 610–619, May 1993.
5. Sabetfakhri, K., and L. P. B. Katehi, "Analysis of integrated millimeter-wave and submillimeter-wave waveguides using orthonormal wavelet expansions," *IEEE Trans. Microwave Theory Tech.,* Vol. 42, No. 12, 2412–2422, Dec. 1994.
6. Wang, G., and G. Pan, "Full wave analysis of microstrip floating line structures by wavelet expansion method," *IEEE Trans. Microwave Theory Tech.,* Vol. 43, No. 1, 131–142, Jan. 1995.
7. Wagner, R. L., and W. C. Chew, "A study of wavelets for the solution of electromagnetic integral equations," *IEEE Trans. Antennas Propag.,* Vol. 43, No. 8, 802–810, Aug. 1995.
8. Xiang, Z., and Y. Lu, "An adaptive wavelet transform for solutions of EM integral equations," *Proc. IEEE Antennas Propagat. Soc. Int. Symp.,* 1104–1107, Montreal, Canada, July, 1997.
9. Xiang, Z., and Y. Lu, "An effective wavelet matrix transform approach for efficient solutions of electromagnetic integral equations," *IEEE Trans. Antennas Propag.,* Vol. 45, No. 8, 1205–1213, 1997.
10. Xiang, Z., and Y. Lu, "An effective hybrid method for EM scattering from inhomogeneous objects," *Progress in Electromagnetic Research*, *PIER 17*, 301–317, 1997.
11. Daubechies, I., *Ten Lectures on Wavelets,* Philadelphia, PA: Society for Industrial and Applied Mathematics, 1992.

12. Chui, C. K., *An Introduction to Wavelets,* Boston MA: Academic Press, 1992.
13. Chui, C. K., and J. Wang, "On compactly supported spline wavelets and a duality principle," *Trans. Amer. Math. Soc.,* Vol. 330, 903–915, 1992.
14. Mallat, S. G., "A theory for multiresolution signal decomposition: the wavelet representation," *IEEE Trans. Pattern Anal. Mach. Intell.,* Vol. 11, 674–693, July 1989.
15. Schoenberg, I. J., *Cardinal Spline Interpolation,* CBMS-NSF Series in Appl. Math. # 12, SIAM Publ., Philadelphia, 1973.